Modeling of the Electronic Properties of Vertical Quantum Dots by the Finite Element Method

Philippe Matagne[1], **Jean-Pierre Leburton**[2], **Jacques Destine, Guy Cantraine**[3]

Abstract: We investigate the quantum mechanical properties and single-electron charging effects in vertical semiconductor quantum dots by solving the Schrödinger and Poisson (SP) equations, self-consistently. We use the finite element method (FEM), specifically the Bubnov-Galerkin technique to discretize the SP equations. Owing to the cylindrical symmetry of the structure, the mesh is generated from hexahedral volume elements. The fine details of the electron spectrum and wavefunctions in the quantum dot are obtained as a function of macroscopic parameters such as the gate voltage, device geometry and doping level. The simulations provide comprehensive data for the analysis of the experimental data of Tarucha, Austing, Honda, van der Hage, and Kouwenhoven (1996).

keyword: quantum dot, finite element, single-electron charging.

1 Introduction

During the last ten years, single electronics has undergone considerable development, driven by the discovery of novel physical effects with potential applications as ultrasmall memories [Imamura, Sugiyama, Nakata, Muto, and Yokoyama (1995); Wasshuber, Kosina, and Selberherr (1998); Likharev (1995); Korotkov (1996)], ultradense digital logic circuits [Meir (1995); Tucker (1992); Korotkov (1996); Likharev (1995)], high efficiency lasers [Fafard, Hinzer, Raymond, Dion, Feng, and Charbonneau (1996)], metrology [Kouwenhoven, Marcus, Mceuen, Tarucha, Westervelt, and Wingreen (1997); Likharev (1995)] and optical detectors [Jimenez, Fonseca, Brady, Leburton, Wohlert, and Cheng (1997); Likharev (1995)]. The most prominent of these effects are single electron charging and Coulomb blockade in tunnel junctions whose size is of the order of the de Broglie wave length ($\leq 50nm$).

Although the latter phenomena were already observed in thin metallic films as early as 1950 [Gorter (1951)], single electronics gained popularity only in the mid eighties with the developement of the so-called 'orthodox theory' by Averin and Likharev (1986). This theory was successfull in explaining single electron effects in metal tunnel junctions where quantum effects such as the discreteness of energy levels do not play an important role. However, in recent experiments on semiconductor quantum dots (QD), features such as single electron orbital motion, three-dimensional energy quantization and shell structures typical to real atoms have been observed [Ashoori, Störmer, Weiner, Pfeiffer, Baldwin, and West (1993, 1994); Tarucha, Austing, and Honda (1995); Tarucha, Austing, Honda, van der Hage, and Kouwenhoven (1996); Tarucha, Austing, and Honda (1997); Kouwenhoven, Oosterkamp, Danoesastro, Eto, Austing, Honda, and Tarucha (1997); Schmidt, Haug, von Klitzing, Förster, and Lüth (1997)]. For these reasons, QDs are often called artificial atoms [Kastner (1993); Lee, Rao, Martin, and Leburton (1998); Leburton and Nagaraja (1997); Jefferson and Häusler (1997); Ashoori, Störmer, Weiner, Pfeiffer, Baldwin, and West (1993)].

The first experiments on single electron charging and Coulomb blockade in semiconductor QDs were made with planar structures by patterning several metal gates above the surface of a two-dimensional electron gas (2DEG) which isolates electrostatically a small region of the 2DEG and forms a QD [Meirav, Kastner, and Wind (1990); Kouwemhoven, Johnson, van der Vaart, and Harmans (1991); Wang and Chou (1993)]. However, the tunneling barriers which confine the electrons in the planar QD have a variable shape which is strongly influenced by the gate voltage [Meirav and Foxman (1995)]. In vertical quantum dots (VQD), the zero-dimensional region is sandwiched vertically between a double resonant tunneling barrier made of heterostructure layers, and lateral confinement is achieved by deep mesa etching. This pillar structure is covered by a metal gate which forms an adjustable Schottky barrier to control the number of electrons in the QD. In addition to the single electron charging effect, Tarucha and coworkers observed that shell filling in vertical QD is governed by Hund's rule, just as in atoms [Tarucha, Austing, Honda, van der Hage, and Kouwenhoven (1996); Tarucha, Austing, and Honda (1997)].

In this paper, we investigate the electronic properties of VQDs which involves the self-consistent numerical solution of Poisson and Schrödinger equations. In recent years, attempts have

[1] Philippe Matagne is PHD student in Electrical Engineering at the Montefiore Institute, University of Liège, Belgium, and visitor at the Beckman Institute for Advanced Science & Technology, University of Illinois at Urbana-Champaign.

[2] Jean-Pierre Leburton is Professor in the de partment of Electrical & Computer Engineering at the University of Illinois at Urbana-Champaign and at the Beckman Institute for Advanced Science & Technology.

[3] Jacques Destiné and Guy Cantraine are Professors in the department of Electrical & Computer Engineering at the Montefiore Institute, University of Liège, Belgium.

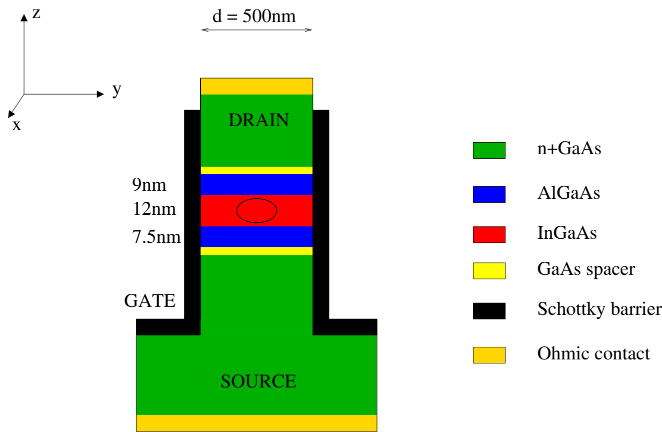

Figure 1 : Schematic diagram of a vertical quantum dot tunnelling heterostructure showing the different semiconductor layers

been made to simulate QD numerically [Macucci, Hess, and Iafrate (1993, 1995); Stopa (1996); Lee, Rao, Martin, and Leburton (1998); Jovanovic and Leburton (1994); Leburton and Nagaraja (1997); Nagaraja, Matagne, Thean, Leburton, Kim, and Martin (1997)], but were of limited validity because simulations were either restricted to two dimensions in order to decrease the computations [Macucci, Hess, and Iafrate (1993, 1995)], or assumed a parabolic background potential [Macucci, Hess, and Iafrate (1993, 1995); Lee, Rao, Martin, and Leburton (1998)], or even neglected spin effects [Jovanovic and Leburton (1994); Leburton and Nagaraja (1997); Nagaraja, Matagne, Thean, Leburton, Kim, and Martin (1997)]. Therefore, there is a need for a comprehensive model which incorporates all the detailed features of the experiment [Tarucha, Austing, Honda, van der Hage, and Kouwenhoven (1996)]. For this purpose, we have developed a realistic model which accounts for the influence of parameters such as the doping, the dimension of the gate or the pinning of the conduction band at the interfaces on the electronic structure of the QD, and directly relates the variation of the microscopic properties of the nanostructure to the macroscopic variations of the applied bias.

We use the finite element method (FEM) to discretize Poisson and Schrödinger equations because this method has the ability to treat complex geometries and a strong mathematical background.

2 Vertical tunneling structures.

Fig. 1 shows a schematic diagram of a vertical QD similar to the device investigated by Tarucha, Austing, and Honda (1995); Tarucha, Austing, Honda, van der Hage, and Kouwenhoven (1996); Tarucha, Austing, and Honda (1997); Austing, Honda, and Tarucha (1996a,b); Kouwenhoven, Marcus, Mceuen, Tarucha, Westervelt, and Wingreen (1997). The structure consists of an undoped $12nm\ In_{0.05}Ga_{0.95}As$ well and undoped $Al_{0.22}Ga_{0.78}As$ barriers of thickness $9nm$ and $7.5nm$. This difference in the barrier thickness is required to facilitate accumulation of electrons in the dot. The inclusion of indium in the well lowers the bottom of the conduction band and circumvents the drawbacks of delta doped $AlGaAs$ barriers of earlier devices [Tarucha, Austing, and Honda (1995)]. The lead on the side of the thinner (thicker) tunnel barrier is made of n^+GaAs and is referred to as the *source* (*drain*). The doping is gradualy reduced from the source (drain) to the double barrier heterostructure (DBH). The DBH is etched to form a circular mesa with a geometrical diameter of the top contact of $0.5\mu m$. A circular Schottky gate surrounding the mesa controls the number of electrons in the dot. Experimental mesurements were made with samples cooled in a dilution refrigerator and the electron temperature was estimated to be about $0.2K$. The current flowing through the dot is measured in response to a small dc voltage ($150\mu V$) applied between the source and the drain. The number of electrons in the dot was determined by tracking the current peaks of the $I-V_{\mathrm{GATE}}$ characteristics.

3 Model

Since the voltages applied between source and drain are extremely small (the curent probed is a few pA [Tarucha, Austing, Honda, van der Hage, and Kouwenhoven (1996)]), and since the gate voltage produces no current, the system is considered to be close to equilibrium. Moreover, since the dot is well isolated from the surrouding $3D$ bulk, we define two regions with almost non overlap : a dot region in which quantum effects are predominant and a bulk region in which quantum effects are negligible.

3.1 Bulk region

In regions where quantum effects are neglegible, the electron density is computed by Thomas-Fermi's approximation :

$$n = N_c \frac{2}{\sqrt{\pi}} F_{1/2}(\eta_c) \tag{1}$$

where N_c is the effective density of states in the conduction band, $\eta_c = -\phi + \Delta E_c / U_T$, and $F_{1/2}$ is the Fermi integral [Antia (1993)] which reduces to the Boltzmann factor for non degenerate semiconductors.

3.2 Dot region

The charge density in the QD is obtained by considering the quantum mechanical nature of the charge carriers within the density functional theory to describe many-body effects [Jones and Gunnarsson (1989)]. Inclusion of many-body effects under the density functional formalism into the Schrödinger equation leads to what is called the Kohn-Sham equation. In order to take into account the spin dependence on the electron-electron interaction, two Kohn-Sham equations ,

Table 1 : Conduction band offsets (*GaAs* is the reference material)

heterointerface	conduction band offset
$GaAs/Al_{0.22}Ga_{0.78}As$	0.181 eV
$GaAs/In_{0.05}Ga_{0.95}As$	−0.05 eV

one for spin up and one for spin down, are solved simultaneously :

$$H^{\uparrow}(\mathbf{r})\psi_m^{\uparrow}(\mathbf{r}) = \varepsilon_m^{\uparrow}\psi_m^{\uparrow}(\mathbf{r}) \qquad H^{\downarrow}(\mathbf{r})\psi_m^{\downarrow}(\mathbf{r}) = \varepsilon_m^{\downarrow}\psi_m^{\downarrow}(\mathbf{r}) \tag{2}$$

where ε_m and ψ_m are the corresponding eigenenergies and eigen states of the hamiltonians $H^{\uparrow}$ and $H^{\downarrow}$:

$$H^{\uparrow(\downarrow)}(\mathbf{r}) = -\frac{\hbar^2}{2}\nabla\left[\frac{1}{m^*(\mathbf{r})}\nabla\right] - q\phi(\mathbf{r}) + \Delta E_c + \mu_{xc}^{\uparrow(\downarrow)}(n) \tag{3}$$

where $m^*(\mathbf{r})$ is the position dependent effective mass. $\phi(\mathbf{r}) = \phi_{ext} + \phi_{ion} + \phi_H$ is the electrostatic potential which consists of three contributions : ϕ_{ext} potential due to external applied bias, ϕ_{ion} potential resulting from ionized donors and ϕ_H Hartree potential accounting for the repulsive electron-electron interactions. ΔE_c is the conduction band offset between different materials (Tab. 3.2) and $\mu_{xc}^{\uparrow(\downarrow)}$ is the exchange and correlation potential energy for spin up($\uparrow$) and down ($\downarrow$) which is computed within the Local Spin Density Approximation (LSDA) according to Perdew and Wang's formulation [Wang and Chou (1993)]. The LSDA approach to the study of electronic structure of quantum dots has been well tested by many authors [Jovanovic and Leburton (1994); Fonseca, Jimenez, Leburton, and Martin (1997); Macucci, Hess, and Iafrate (1993); Stopa (1996)]. It successfully explains the quasi two-dimensional shell structures and spin configurations of quantum dots [Tarucha, Austing, Honda, van der Hage, and Kouwenhoven (1996); Tarucha, Austing, and Honda (1997)]. Moreover, applications of the LSDA to few electron atoms has shown accuracy of the order of 1% in the calculations of the atoms ionisation energy [Jones and Gunnarsson (1989)].

The electron density in the QD reads

$$n(\mathbf{r}) = n^{\uparrow}(\mathbf{r}) + n^{\downarrow}(\mathbf{r}) = \sum_{i=1}^{N_{\uparrow}}\left|\psi_m^{\uparrow}(r)\right|^2 + \sum_{i=1}^{N_{\downarrow}}\left|\psi_m^{\downarrow}(r)\right|^2 \tag{4}$$

where $N_{\uparrow} + N_{\downarrow} = N$ is the number of electrons in the dot.

The electrostic potential $\phi(\mathbf{r})$ is computed by solving Poisson equation :

$$\nabla(\varepsilon(\mathbf{r})\nabla\phi(\mathbf{r})) = -\rho(\mathbf{r}) \tag{5}$$

where $\varepsilon(\mathbf{r})$ is the position dependant permittivity and $\rho(\mathbf{r})$ is the total charge density which is given by

$$\rho(\mathbf{r}) = q(p(\mathbf{r}) - n(\mathbf{r}) + N_D^+(\mathbf{r}) - N_A^-(\mathbf{r})) \tag{6}$$

where $p(\mathbf{r})$, $n(\mathbf{r})$, $N_D^+(\mathbf{r})$, $N_A^-(\mathbf{r})$ are the hole, electron, ionized donnors and ionized acceptors densities respectively, at the position $\mathbf{r}$.

3.3 Boundary conditions

Boundary conditions for the electrostatic potential ϕ are chosen by imposing Dirichlet conditions at the source, drain and lateral surfaces of the device. At the source and drain, flat band condition is assumed and ϕ is set up such that the net charge is zero in these regions. Along lateral surfaces, the Schottky barriers heights ϕ_s are strongly influenced by surface chemistry, so we use the experimental data of Grant, Waldrop, Kowalczyk, and Kraut (1981) and Best (1979). On the gated surfaces, the Schottky barriers are modified by $\phi_s - V_G$, where V_G is the gate bias.

Boundary conditions for the Khon-Sham's equation are imposed by assuming vanishing wave functions on any lateral surface of the device. Since the quantum dot is much smaller than the physical dimensions of the device, the wave functions vanish actually far away from those boundaries. In the direction perpendicular to the hetero-interfaces, we allow wave functions to leak into the source and drain regions. However, this leakage is not taken into account for the computation of the charge in the source and drain regions where it is computed entirely using the Thomas-Fermi approximation in that region. This is a good approximation since it doesn't affect the charge within the dot, and is too small compared to the bulk charge in the source and drain regions.

3.4 Single electron charging

Because the quantum dot is weakly coupled to the source and drain, electrons are completely localized in the dot At equilibrium, and for a given bias, the integer number of electrons N minimizes the total energy E_T of the system. In order to determine N we use the Slater formula [Slatter (1972)]:

$$E_T(N+1) - E_T(N) = \int_0^1 \varepsilon_{LUO}(n)dn \approx \varepsilon_{LUO}(1/2) \tag{7}$$

where $E_T(N)$ is the total energy for N electrons in the dot and ε_{LUO} is the lowest unoccupied orbital eigenvalue. Hence, upon populating ε_{LUO} with 0.5 electron, a stable configuration of N electrons is achieved in the dot if $E_T(N+1) > E_T(N)$, i.e. if the integral of Eq.7 is positive, otherwise there are $N+1$ electrons. It must be noted that the approximation made in Eq. 7 is valid only if ε_{LUO} varies linearly with N. Calculations of Fonseca, Jimenez, Leburton, and Martin (1997) have established the validity of the approximation in self-assembled $InAs/GaAs$ quantum dots.

4 Mesh generation

Fig. 2 shows the mesh generated for the cylindrical DBH. As mentioned before, the volume of the device is divided into hexahedra, some of which, however, may degenerate into prisms.

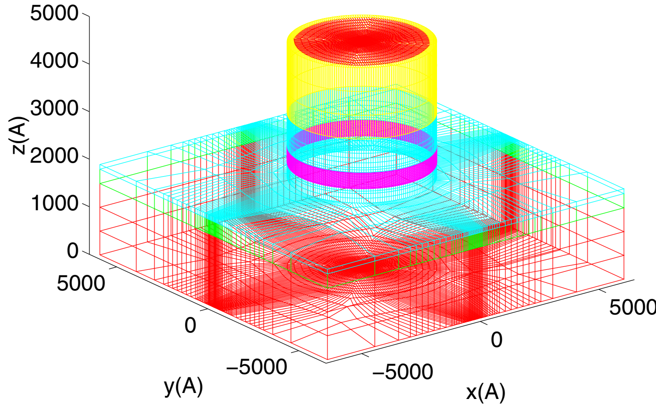

Figure 2 : Hexahedral elemental mesh for a cylindrical DBH

Along the vertical direction, the mesh is refined gradually from the source and drain to the heterointerfaces. In the horizontal plane, a irregular square mesh is first generated. Again, it is refined gradually from the perimeter to the center. If $a^s_{ij} = (x^s_i, y^s_j)$ is a point on this square mesh, the corresponding point $a^c_{ij} = (x^c_i, y^c_j)$ in the circular mesh of radius R is computed by the transformation :

$$x^c_i = r\,\Xi\,cos(\theta)\,sign(x) + x^s_i\,(1-\Xi) \tag{8}$$

$$y^c_j = r\,\Xi\,sin(\theta)\,sign(y) + y^s_j\,(1-\Xi) \tag{9}$$

$$\begin{array}{llll} where \quad r & = & max(|x^s_i|, |y^s_j|) & \\ \theta & = & \frac{|j|\,\pi}{4|i|} & (|x_s| \geq |y_s|) \\ & & \frac{2|j|-|i|}{4|j|} & (|x_s| \leq |y_s|) \\ \Xi & = & \frac{max(|i|,|j|)}{R_n} & (r \leq R) \\ & & \frac{n-max(|i|,|j|)}{n-R_n-1} & (r > R) \\ i,j & \in & [-n..n] & \end{array} \quad \text{and } (R_n+1)$$

is the number of grid points spanned by R. Because of this transformation, when $r = R$, $\Xi = 1$ and Eq. 9 are coordinates of points lying on the circumference of radius R. When $r \ll R$, $\Xi \approx 0$, the first term of the sum in the right hand side of Eq. 9 almost vanishes and $a^c_{ij} \approx a^s_{ij}$ When $r = n$, $\Xi = 0$ and Eq. 9 are coordinates of points lying on the perimeter of the buried region. Thus, as seen in Fig. 2, the mesh is almost square in the inner part of the device and becomes circular gradually away from the center to fits exactly the surface of the cylinder and becomes square again in order to fit the surface of the parallelipipedic lower part of the device.

5 Finite element formulation

In the present work, Poisson and Kohn-Sham equations are discretized by the FEM, more precisely by the *Bubnov-Galerkin* method [Zienkiewicz and Taylor (1994)]. The electrostatic potential and the wave functions are approximated by piecewise trilinear polynomials on isoparametric hexahedral elements.

5.1 *Reference finite element*

We define our reference finite element by the triplet (K, P, S) [Brenner and Scott (1994)] where

- the element domain K is the cube whose vertices are α_1(-1,-1,-1), α_2(1,-1,-1), α_3(-1, 1,-1), α_4(1, 1,-1), α_5(-1,-1, 1), α_6(1,-1, 1), α_7(-1, 1, 1), α_8(1, 1, 1) (local coordinates)
- P is the restriction on K of trilinear polynomials. : $P = \{\sum_j c_j p_j(\xi) q_j(\eta) r_j(\zeta)\,:\, p_j, q_j, r_j$ linear polynomials $\}$
- the nodal variables $S = \{\alpha_1, \alpha_2, \alpha_3, \alpha_4, \alpha_5, \alpha_6, \alpha_7, \alpha_8\}$

It can easily be shown that $\{N_1, N_2, N_3, N_4, N_5, N_6, N_7, N_8\}$ defined by

$$N_i(\xi, \eta, \zeta) = \frac{1}{8}(1 \pm \xi)(1 \pm \eta)(1 \pm \zeta) \quad i = 1 \ldots 8 \tag{10}$$

is a basis for P. Now, any hexahedral element (K_e, P_e, S_e) whose vertices are $\{a_1, a_2, a_3, a_4, a_5, a_6, a_7, a_8\}$ where $a_i = (x_i, y_i, z_i)$ (global coordinates) can be related to the reference element via the isoparametric transformation :

$$a = \mathbf{N}^{\mathbf{T}}\mathbf{C} \tag{11}$$

where $a = (x, y, z)$ is any coordinate in K_e, $\mathbf{N}$ is the column vector of basis functions and $\mathbf{C}$ is a 8×3 matrix whose i^{th} row is the vertex (x_i, y_i, z_i).

5.2 *Poisson equation*

In the finite element method we have to discretize the weak form of Poisson equation :

$$\int_\Omega \varepsilon(\mathbf{r})\ \nabla\phi(\mathbf{r}).\nabla W(\mathbf{r})\ d\mathbf{r} = \int_\Omega \rho(\phi)\ W(\mathbf{r})\ d\mathbf{r} + \int_{\Sigma_0} \varepsilon(\mathbf{r})\ \nabla\phi(\mathbf{r}) W(\mathbf{r})\ d\mathbf{r} \tag{12}$$

that we obtain by multiplying Eq. 5 by $W \in H^1$ (*Sobolev* space), integrating over the volume Ω of the structure and applying Green's formula. Σ denotes the surface of the device with $\Sigma = \Sigma_0 \cup \Sigma_1$ where, as discussed before, $\phi(\mathbf{r}) = \phi_0(\mathbf{r})$ on Σ_0 (Dirichlet boundary condition) and $\nabla\phi(\mathbf{r}) = 0$ on Σ_1 (Neumann boundary condition).

Discretization of Eq. 12 is performed choosing $W = N_i \in P \subset H^1$ and, in each element, replacing ϕ by its interpolant :

$$\tilde{\phi} = \sum_{i=1}^{8} N_i \phi_i \tag{13}$$

After some algebra, Eq. 12 can be cast into a matrix form:

$$\mathbf{Q}\phi = \rho + \mathbf{Q}_0\phi_0 \tag{14}$$

where

$$\mathbf{Q} = \sum_{e=1}^{m} \overline{\mathbf{Q}}^e \quad , \quad \rho = \sum_{e=1}^{m} \overline{\rho^e} \quad , \quad \mathbf{Q}_0 = \sum_{e=1}^{m} \overline{\mathbf{Q}}_0^e$$

$$Q_{ij}^e = \int_{-1}^{1}\int_{-1}^{1}\int_{-1}^{1} \varepsilon \nabla N_i(\mathbf{r}(\xi,\eta,\zeta))\nabla N_j(\mathbf{r}(\xi,\eta,\zeta)) \times |J|\, d\xi\, d\eta\, d\zeta, \tag{15}$$

$$\rho_i^e = \int_{-1}^{1}\int_{-1}^{1}\int_{-1}^{1} \rho(\tilde{\phi})\, N_i(\mathbf{r}(\xi,\eta,\zeta))\, |J|\, d\xi d\eta d\zeta, \tag{16}$$

$\overline{Q}_{ij}^e = Q_{ij}^e$ if Q_{ij}^e does exist, and 0 otherwise (the same definition applies for $\overline{\rho}_i^e$). $\mathbf{Q}$ is a $n \times n$ matrix and ϕ is a n row vector of unknown nodal potential. $\mathbf{Q}_0$ is a $n \times n_0$ matrix and ϕ_0 is a n_0 row vector denoting the Dirichlet boudary condition. The summation is performed over the m finite elements of the mesh. In three-dimensional problems, n^2 becomes quickly a very large number. Fortunately, $\mathbf{Q}$ is sparse and only the non zero elements are stored in memory. Actually, each row of $\mathbf{Q}$ contains 27 non zero elements since in hexahedral finite elements, each node is related to its 26 neighbours.

In order to get Eq. 15 and 16, we have applied the change of variable described by Eq. 11. Therefore, except the Jacobian J, Eq. 15 and Eq. 16 are independent of any particular element, Ω^e, which reduces significantly the programming effort. It must also be noted that ε is constant in Ω^e because an element is related to one material.

Since ρ depends on ϕ, Eq. 14 is a nonlinear equation that is solved iteratively by the damped *Newton-Raphson* method :

$$\begin{cases} J\Delta\phi^{(l+1)} = -\mathbf{F}^{(l)} \\ \phi^{(l+1)} = \phi^{(l)} + \alpha\, \Delta\phi^{(l+1)} \end{cases} \tag{17}$$

where

$$\begin{aligned} \mathbf{F} &= \mathbf{Q}\phi - \rho - \mathbf{Q}_0\phi_0 \\ J_{ij} &= \frac{\partial F_i}{\partial \phi_j} = Q_{ij} - \frac{\partial \rho_i}{\partial \phi_j} \end{aligned} \tag{18}$$

and l is the number of the iteration and J , the Jacobian matrix. The damping factor α is set up by a incomplete line search. From Eq. 15, it is obvious that $\mathbf{Q}$ is symmetric and positive definite. In order to maintain the symetry of J, we only consider the diagonal part of $\left(\frac{\partial \rho_i}{\partial \phi_j}\right)$. Since J is a sparse matrix, we use the conjugate gradient method to solve Eq. 17 and iterate until $\max_i |\Delta\phi_i| < tol$ (we have fixed $tol = 10^{-6} eV$).

5.3 *Kohn-Sham equation*

The weak form of Kohn-Sham equation reads :

$$\int_\Omega \frac{\hbar^2}{2m^*}(\nabla\psi_m(\mathbf{r})).\nabla W(\mathbf{r})\, d\mathbf{r} = \int_\Omega (\varepsilon_m - U(\mathbf{r}))W(\mathbf{r})\, \psi_m\, d\mathbf{r} \tag{19}$$

where $U(\mathbf{r}) = E_c(\mathbf{r}) + \mu_{xc}(n)$. Since the boundary conditions are $\psi = 0$ on Σ_0 and $\nabla\psi = 0$ on Σ_1, there is no surface term in Eq. 19. Applying the same procedure as in Poisson equation, we get, after discretization :

$$\mathbf{H}^e\psi_m^e = \mathbf{A}^e\psi_m^e + \mathbf{B}^e\psi_m^e = \varepsilon_m \mathbf{M}\psi_m^e \tag{20}$$

where

$$A_{ij}^e = \int_{-1}^{1}\int_{-1}^{1}\int_{-1}^{1} \frac{\hbar^2}{2m^*} \nabla N_i(\mathbf{r}(\xi,\eta,\zeta))\nabla N_j(\mathbf{r}(\xi,\eta,\zeta)) \times |J|\, d\xi\, d\eta\, d\zeta \tag{21}$$

$$B_{ij}^e = \int_{-1}^{1}\int_{-1}^{1}\int_{-1}^{1} U(\mathbf{r}(\xi,\eta,\zeta))\, N_i(\mathbf{r}(\xi,\eta,\zeta))\, N_j(\mathbf{r}(\xi,\eta,\zeta)) \tag{22}$$

$$\times |J|\, d\xi\, d\eta\, d\zeta \tag{23}$$

$$M_{ij}^e = \int_{-1}^{1}\int_{-1}^{1}\int_{-1}^{1} N_i(\mathbf{r}(\xi,\eta,\zeta))\, N_j(\mathbf{r}(\xi,\eta,\zeta)) \tag{24}$$

$$\times |J|\, d\xi\, d\eta\, d\zeta \tag{25}$$

Assembling the parts, we get

$$\mathbf{H}\psi_m = \varepsilon_m \mathbf{M}\psi_m \tag{26}$$

Whereas $\mathbf{A}$ is positive definite, $\mathbf{H}$ may not be so since it depends on U which can take any value. In order to keep the symetry and definite positiveness of the problem, we solve the following equation instead of Eq. 20:

$$\mathcal{H}\psi_m = \lambda_m \mathbf{M}\psi_m \tag{27}$$

where $\mathcal{H} = \mathbf{H} - U_{min}\mathbf{M}$ is symetric definite positive and $\lambda_m = \varepsilon_m - U_{min}$.

To find the lowest S occupied eigenstates, we must solve the general eigenvalue problem

$$\mathcal{H}\Psi = \mathbf{M}\Psi\Lambda \tag{28}$$

where Ψ is $n' \times S$, $\mathcal{M}$ an orthogonal matrix whose m^{th} column holds ψ_m and n', the unknown number of the dot region ($n' \leq n$). This system is solved by a subspace iteration method based on a Rayleigh-Ritz analysis whose algorithm is a variation of the one described in [Bathe (1996)].

The solution involves :

(a) Choosing a set S of linearly independent vectors as an initial guess for the basis of the subspace : $\overline{\psi}_1, \ldots, \overline{\psi}_S$

(b) Performing a Rayleigh quotient iteration,

$$\left(\mathcal{H} - \frac{\Psi_1^T K \Psi_1}{\Psi_1^T \mathbf{M}\Psi_1}\mathbf{M}\right)\overline{\Psi} = \mathbf{M}\Psi$$

(c) Finding the projections of $\mathcal{H}$ and $\mathbf{M}$ onto the subspace, i.e.,

$$\mathcal{H}_S = \overline{\Psi}^T\left(\mathcal{H} - \frac{\Psi_1^T K \Psi_1}{\Psi_1^T \mathbf{M}\Psi_1}\mathbf{M}\right)\overline{\Psi} \quad , \quad \mathbf{M}_S = \overline{\Psi}^T\mathbf{M}\overline{\Psi}$$

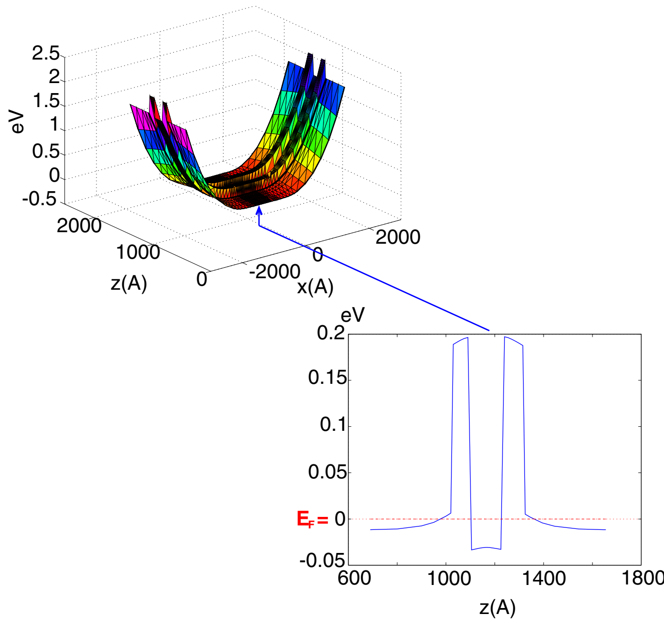

Figure 3 : Conduction band profile in the xz plane (growth direction) at $y = 0$ for 20 electrons in the dot ($V_G = -0.61V$). The inset shows a cross section at $x = 0$

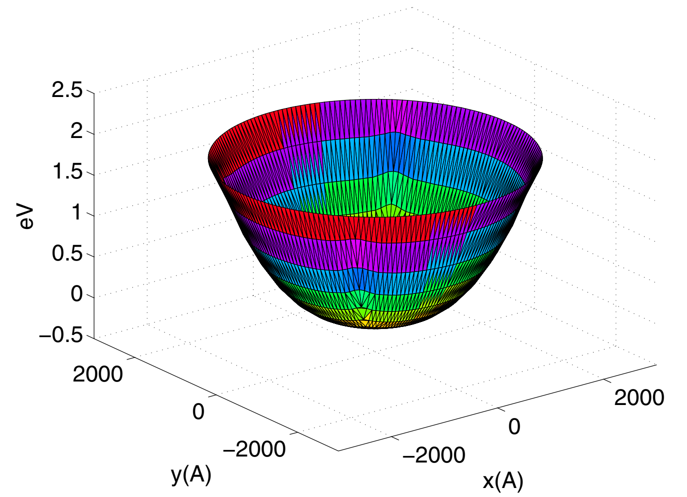

Figure 4 : Conduction band profile in the xy plane for 0 electron in the dot ($V_G = -1.7V$) at $y = 0$ and $z = 1180Å$

(d) Using the QR method, finding the S eigenvalues and eigenvectors of this reduced system,

$$H_S \Psi_S = \mathbf{M}_S \Psi_S \Lambda_S$$

(e) Building an improved basis using linear combinations of the eigenvectors of the subspace

$$\Psi = \overline{\Psi} \Psi_S$$

(f) repeating steps (b) through (e) until $\max_i |\frac{\lambda_i^{(k+1)} - \lambda_i^{(k)}|}{\lambda_i^{(k)}}| < tol$, where k is the iteration number.

Step (b) insures cubic convergence to ψ_1 and the convergence rate to ψ_i $(i = 2, \ldots, S)$ is λ_i/λ_S [Bathe (1996)]. Since $S \ll n'$, the number of operations required for step (c) ($o(S^3)$) can be neglected and the total number of operations is $o(13^2 n')$ [Bathe (1996)]. It can be proved [Bathe (1996)] that step (d) improves the solution and eventually, Λ_S converges to the S lowest eigenvalues of H. Although not the fastest possible, this method is very robust and avoids propagation of round off errors occuring in all the Gram-Schmidt based methods. Moreover, the algorithm finds all the eigenvalues in the subspace without exhibiting any unstable behaviour in the case of degeneracies.

6 Results

Fig. 3 shows the variation of the conduction band edge $E_C(\mathbf{r}) = \Delta E_C - q\phi + \mu_{xc}$ including many-body effects in the xz-plane at $y = 0$, i.e. in the dot, for $N = 20$ electrons ($V_G = -0.61V$). The source and drain regions have been excluded from the figure since there are no significant potential variations in these regions. The inset shows a cross-section at $x = 0$. The central *InGaAs* dot region ($1030Å \leq z \leq 1315Å$) is defined by the $180meV$ *AlGaAs* double barrier. The lower energy gap of *InGaAs* ($1.448eV$) compared to the energy gap of *GaAs* ($1.519eV$) results in the bottom of the well being $50meV$ lower than the source and drain regions. Therefore, electrons are confined in the $120Å$ wide *InGaAs* region.

Fig. 4 shows the variation of the conduction band edge in the xy plane at $z = 1180Å$, i.e., in the well, for $N = 0$. It confirms the parabolic shape of the conduction band in this region, as well as the cylindrical symmetry of the structure.

Fig. 5 shows the variation of the conduction band edge $E_C(\mathbf{r})$ along the x direction, perpendicular to the growth direction, at $y = 0$ and $z = 1180Å$, i.e. in the quantum dot, for N varying from 0 to 20, i.e. $-1.7V < V_G < -0.61V$. It is seen that when the dot is empty, the conduction band profile is almost parabolic, but as the gate voltage is varied, thus increasing the number of electrons in the dot, the bottom of the conduction band flattens, due to increasing Coulomb repulsion (Hartree potential) between charge carriers. The inset shows that the minimum of the conduction band edge $E_C(\mathbf{r})$ in the dot is not a monotonic function of the number of electrons N, but oscillates as a combined influence of the attractive ion potential ϕ_{ION} and μ_{xc}, and the repulsion between electrons ϕ_H.

Fig. 6 shows the electron concentration, $n(\boldsymbol{r})$ in the xz plane at $y = 0$, for $N = 20$. The effect of the different types of confinements is evident in the figure : Along the z-direction, the electrons in the dot are squeezed into a thin layer whereas in the x-direction, the concentration profile is more spread out and

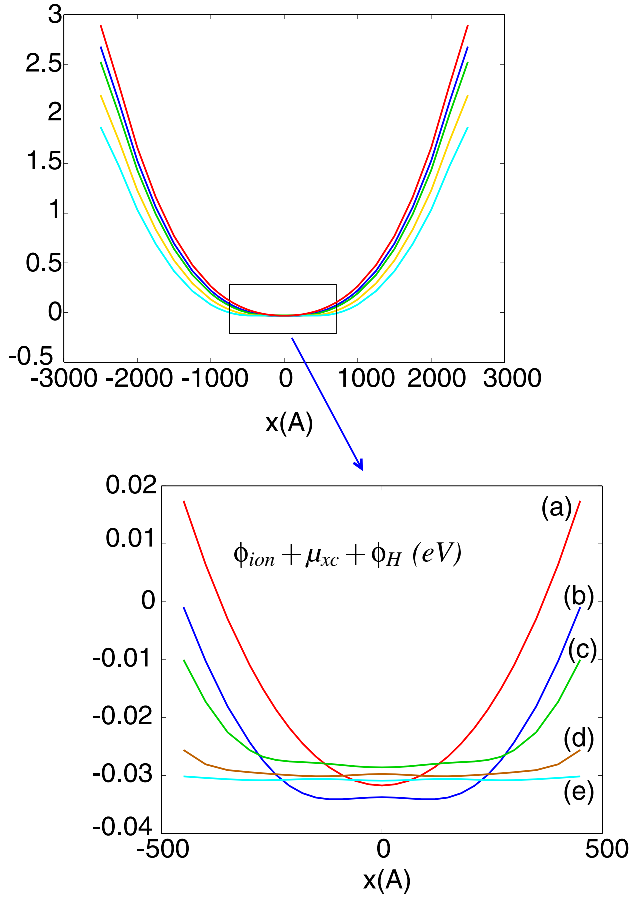

Figure 5 : Conduction band profile in the x direction (perpendicular to the growth direction) at $y = 0$ and $z = 1180Å$, i.e., in the quantum well for N equals (a) 0 ($V_G = -1.7V$), (b) 2 ($V_G = -1.56V$), (c) 6 ($V_G = -1.2V$), (d) 12 ($V_G = -0.9V$) and 20 ($V_G = -0.609V$) electrons. The inset is a zoom of the box drawn in the general view.

exhibits four lobes, which results from the contributions of the occupied excited states The only lobe along the z-direction indicates that only the ground z-state , i.e., $n_z = 0$, is occupied, if we label the states as (n_x, n_y, n_z) where n_x, n_y and n_z are the number of nodes in the x, y and z directions respectively.

As mentioned in the introduction, the spectrum of QD exhibits a shell structure if the potential is characterized by a high level of symmetry, which is the case for this cylindrical structure. Fig. 7 shows the evolution of the eigenvalues as a function of the gate voltage. Because of the parabolic shape of the confining potential in the x and y directions when the dot is empty ($V_G \approx -1.7V$), the eigenvalues achieve a 2D cylindrical harmonic oscillator spectrum.

By analogy with atomic physics, we use $s, p, d, f, \ldots$ for the four lower states with degeneracy $2, 4, 6, 8$, including the spin. The general trends of the energy spectrum is to move to lower energies as the gate voltage is increased since the overall potential energy of the system decreases. A new electron entering the dot induces an upward shift of the whole spectrum due to an sudden increase of the total electrostatic energy in the dot due to electron repulsion. This transition occurs when a particular eigenlevel crosses the Fermi level (zero on the vertical scale) and fulfills the condition $E_T(N+1) < E_T(N)$. This behaviour is different from the results of Nagaraja, Matagne, Thean, Leburton, Kim, and Martin (1997) whose model didn't account for individual spin states. In that case, the eigenvalue was tangential to the Fermi level during the charging of the whole orbital. The intervals ΔV_G between two jumps of the

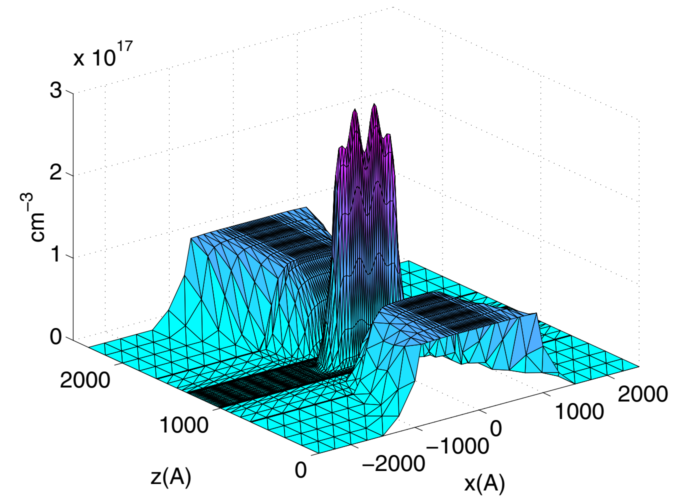

Figure 6 : Electron concentration in the xz plane (growth direction) at $y = 0$ for 16 electrons in the dot.

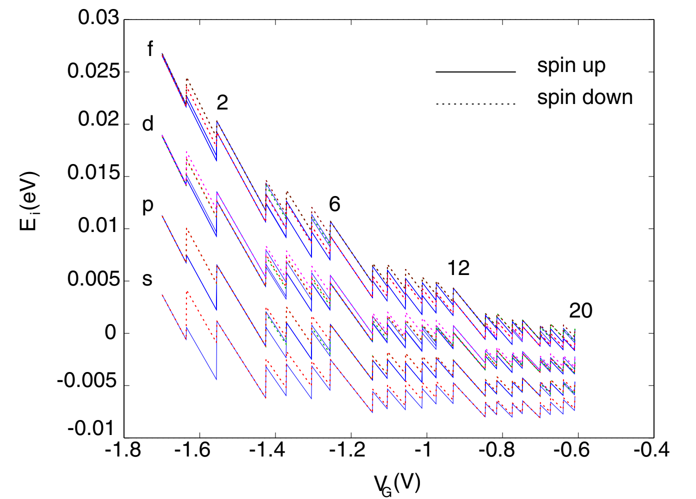

Figure 7 : Eigenlevel spectrum (solid curves : spin up, dotted curves : spin down) as a function of the gate voltage. The labels on the right indicates the first four orbitals, and the numbers at the transitions indicate the number of electrons at the completion of each shell.

energy spectrum represents the increment of V_G, and hence the energy eV_G, required to add an electron to the dot. Unlike in "orthodox" Coulomb blockade experiments [Averin and Likharev (1986)], ΔV_G takes very unequal values, irregularly distributed over the range of V_G, because of the influence of the quantization and quantum many-body effects during the charging of the dot. Hence, after a shell is completely filled, i.e., for $N = 2, 6, 12$ and 20, ΔV_G is usually large because, in addition to the energy required to overcome the electrostatic repulsion of the electrons already present in the dot, an energy contribution is needed to lower the next orbital below the Fermi level for admitting the next electron. However, it is seen that $\Delta V_G^2 = 133meV > \Delta V_G^6 = 111meV > \Delta V_G^{12} = 84meV \ldots$ where ΔV_G^N is ΔV_G for N electrons. This is due to the many-body potential energies ϕ_H and μ_{xc} (equ. 3), which reduce the depth of the overall confining potential (see Fig. 5), and thereby the eigenlevel spacing, when N increases. From atomic physics it is known that the most energetically favorable orbital filling sequence in a particular shell is predicted by Hund's rule. For instance, the charging of the p state follows the spin sequence $2p_x^{\uparrow}, 2p_y^{\uparrow}, 2p_x^{\downarrow}, 2p_y^{\downarrow}$ because the weak overlap between the $2p_x$ and $2p_y$ orbital and the attractive exchange interaction between same spin states favors the $2p_y^{\uparrow}$ over the $2p_x^{\downarrow}$ state which has a strong overlap with the previously filled $2p_x^{\uparrow}$ state, and thereby a bigger repulsive Hartree energy. This explains that the next voltage increments are $\Delta V_G^3(55meV) < \Delta V_G^4(66meV)$, after the large gate voltage increment ΔV_G^2 required for populating the $2p_x^{\uparrow}$ state because of the orbital change. By similar arguments, one can explain the various sizes of the gate voltage increments.

With electrons in the dot, the states of a particular shell are no longer degenerate : for instance, at $V_G = -1.6V$, the d orbital splits and this situation persists, and even emphasizes, at higher V_G. At $V_G = -1.434V$, the p orbital splits into four distinct states while at $V_G = -1.372V$, the p states of same spin merge back together. The orbital degeneracies are lifted for three reasons : first, as it was shown on Fig. 5, the conduction band edge is no longer parabolic due to the influence of the many-body effects, which induces a permanent lifting of degeneracies as occurs for d and f states. Secondly, Hund's rule breaks the symmetry of the shells, lifting temporarly their degeneracy. Hence, after populating the $2p_x^{\uparrow}$ state, the symmetry in the $p^{\uparrow}$ subshell is broken and results in the two $p^{\uparrow}$ levels being clearly separated. After populating the $2p_y^{\uparrow}$ state with the fourth electron, the symmetry in the $p^{\uparrow}$ subshell is restored and the $p^{\uparrow}$ ($p^{\downarrow}$) levels merge back together although the spin degeneracy remains lifted because thirdly, whenever $\mu_{xc}^{\uparrow}$ differs from $\mu_{xc}^{\downarrow}$, the spin degeneracy is lifted. This effects occurs whenever a shell is partially filled because of Hund's rule and the fact that μ_{xc} is a function of the spatial distribution of the electron density. As an exception to this rule the spin degeneracy of the s state remains unaltered for $V_G < -1.434V$ because there is no exchange between the s electrons. The lifting of the

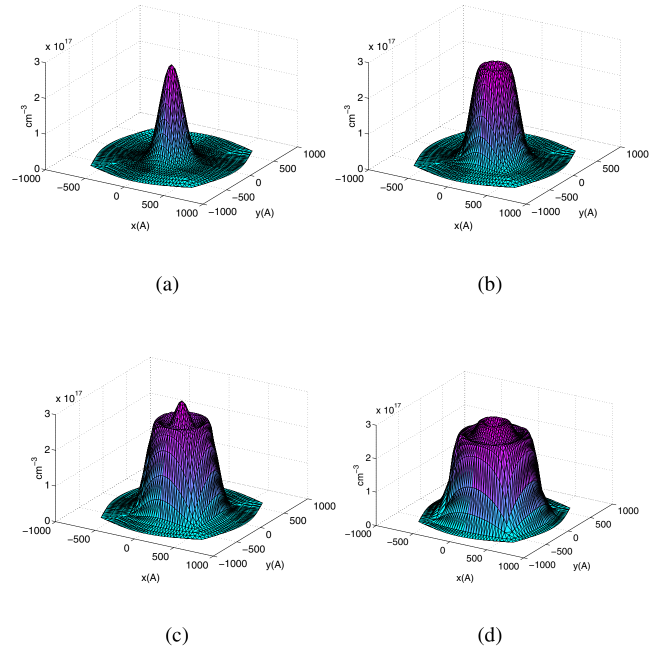

Figure 8 : Electron density profile for (a)2, (b)6, (c)12 and (d)20 electrons in the dot

d and f degeneracies can be explained by the combination of the three effects mentioned above.

Fig. 8 shows the evolution of the electron density $n(\boldsymbol{r})$ in the xy plane as N increases from 2 to 20. Each subplot corresponds to a filled 2D shell. Each density profile can be understood from figure 9 which shows the contour plots of the eigenfunctions where the electron density is equal to the summation of the square of the wave functions over the occupied states. Hence, for two electrons in the dot, i.e., one electron of each spin on the s state (Fig. 8a), the electron density has one lobe and a maximum at the center, which is in agreement with the wavefunction of Fig. 9a. When the p orbital is filled, i.e. $N = 6$, the maximum has moved on a ring around the center (Fig. 8b) since the two p states have a node at the center and two maxima 250$\AA$ away from it (Fig. 9b & c). When the d orbital is completely filled, i.e. $N = 12$, the maximum of $n(\boldsymbol{r})$ moves back to the center, but the crown is still present, although further away from the center (Fig. 8c). This is consistent with Fig. 9d, e and f ; Fig. 9f shows a maximum at the center while Fig. 9d and e have their maximum 280$\AA$ away from it. At last, when the f orbital is filled, i.e. $N = 20$, the maximum of the electron density moves back again at the periphery since all the f wave functions (Fig. 9 g,h,i,j,k,l) have their maximum at the periphery.

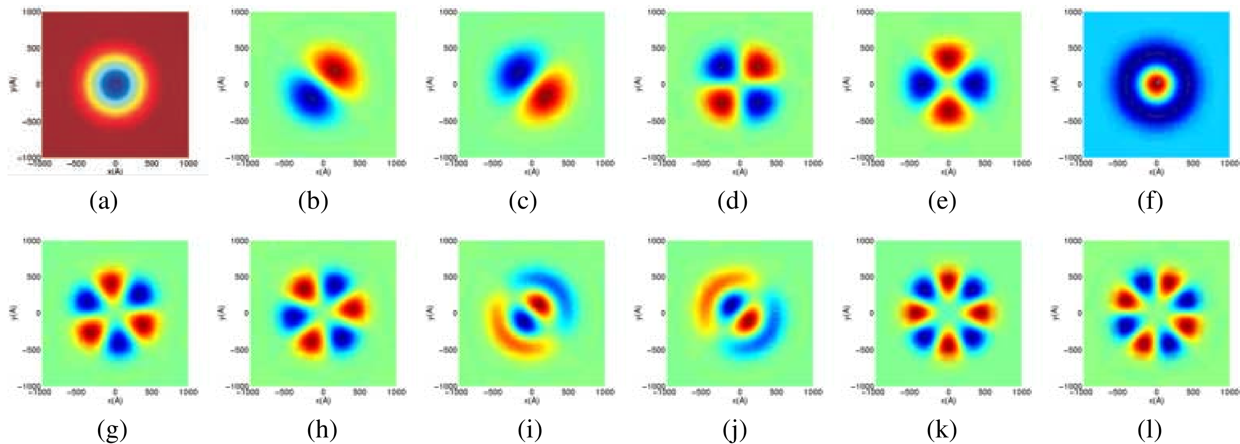

Figure 9 : s(a), p(b,c), d(d,e,f), f(g,h,i,j) and g(k,l) eigenvector contour plots. (n_z has been omitted and is assumed to be 0)

7 Conclusion

Our FEM simulation has successfully reproduced the atomic-like properties of vertical quantum dots. In particular, it has showed the importance of the shell structure and Hund's rules in the charging of the dot. Aside from the good agreement with the experimental data, our model has also been able to provide a comprehensive picture of the detailed evolution of the electronic spectrum as a function of confinement and many-body effects in the dot. This approach has demonstrated the flexibility of the FEM to handle complicated semiconductor structures with basic quantum mechanical effects.

Acknowledgement: We would like to thank S.Nagaraja, A.Thean, S. Tarucha and D. Austing for valuable discussions, and Y.H. Kim for making available the LSDA subroutine. This work is supported by NSF Descartes Grant No. ECS 98-02730, by CRI Grant of the University of Illinois and a special Grant of University of Liège FSA.

References

Abstreiter, G., et al.(Ed): *Optical Spectroscopy of Low Dimensional Semiconductor, NATO ASI Series E*. Kluwer Academic Publisher.

Antia, H. (1993): Rational function approxiamtion for Fermi-Dirac integrals. *The Astrophysical Journal Supplement Series*, vol. 84, pp. 101–108.

Ashoori, R. C.; Störmer, H. L.; Weiner, J.; Pfeiffer, L.; Baldwin, K.; West, K. (1993): N-electron ground state energies of a quantum dot in magnetic field. *Physical Review Letters*, vol. 71, no. 4, pp. 613–616.

Ashoori, R. C.; Störmer, H. L.; Weiner, J.; Pfeiffer, L.; Baldwin, K.; West, K. (1994): Energy levels of an artificial atom probed with single-electron capacitance spectroscopy. *Surface Science*, vol. 305, pp. 558–565.

Austing, D. G.; Honda, T.; Tarucha, S. (1996): A new design for submicron double-barrier resonant tunneling transistors. *Semiconductor Science and Technology*, vol. 11, pp. 388–391.

Austing, D. G.; Honda, T.; Tarucha, S. (1996): Processing and caracteerisation of artificial semiconductor atoms and molecules containing a few electrons.

Averin, D.; Likharev, K. K. (1986): *Journal of Low Temperature Physics*, vol. 62, pp. 345.

Bathe, K.-J. (1996): *Finite Element Procedures*. Prentice Hall.

Best, J. (1979): The Schottky-barrier height of an on $Ga_{1-x}Al_xAs$ as a function $AlAs$ content. *Applied Physics Letters*, vol. 34, pp. 522–524.

Brenner, S. C.; Scott, L. R. (1994): *The Mathemetical Theory of Finite Element Methods*. Springer-Verlag.

Fafard, S.; Hinzer, K.; Raymond, S.; Dion, M.; Feng, J. M. Y.; Charbonneau, S. (1996): Red-emitting semiconductor quantum dot lasers. *Science*, vol. 274, pp. 1350.

Fonseca, L. R.; Jimenez, J. L.; Leburton, J.-P.; Martin, R. M. (1997): Self-consistent calculation of electronic structure and electron-electron interaction in self-assembled InAs-GaAs quatum dot structures. *Physical Review B*.

Gorter, C. (1951): *Physica*, vol. 15, pp. 777.

Grant, R.; Waldrop, J.; Kowalczyk, S.; Kraut, E. (1981): Correlation of GaAs surface chemistry and interface Fermi-level position: a single defect model interpretation. *Journal of Vacuum Science and Technology*, vol. 19, pp. 477–480.

Imamura, K.; Sugiyama, Y.; Nakata, Y.; Muto, S.; Yokoyama, N. (1995): New optical memory structure using self-assembled InAs quantum dots. *Japanese Journal of Applied Physics*, vol. 34, pp. 1445.

Jefferson, J.; Häusler, W. (1997): Quantum dots and artificial atoms. *Condense Materials*.

Jimenez, J. L.; Fonseca, L. R.; Brady, D.; Leburton, J.-P.; Wohlert, D. R.; Cheng, K. (1997): The quantum dot spectrometer. *Applied Physics Letters*, vol. 71, no. 25, pp. 3558.

Jones, R.; Gunnarsson, O. (1989): The density functional formalism, its application and prospects. *Review of Modern Physics*, vol. 61, no. 3, pp. 689–746.

Jovanovic, D.; Leburton, J.-P. (1994): Self-consistent analysis of single-electron charging effects in quantum-dot nanosrtuctures. *Physical Review B*, vol. 49, no. 11, pp. 7474–7483.

Kastner, M. A. (1993): Artificial atoms. *Physics Today*, pg. 24.

Korotkov, A. N. (1996): Coulomb blockade and digital single-electron devices. *Condense Materials*.

Kouwemhoven, L.; Johnson, A.; van der Vaart, N.; Harmans, C. (1991): Quantized currents in a quantum-dot turnstile using oscillating tunnel barriers. *Physical Review Letters*, vol. 67, no. 12, pp. 1626–1629.

Kouwenhoven, L. P.; Marcus, C. M.; Mceuen, P.; Tarucha, S.; Westervelt, R.; Wingreen, N. (1997): *Electron transport in quantum dots*, pp. 105–214. In Sohn, L.L., et al. Sohn, L.L., et al. (1997), 1997.

Kouwenhoven, L. P.; Oosterkamp, T. H.; Danoesastro, M. W.; Eto, M.; Austing, D. G.; Honda, T.; Tarucha, S. (1997): Excitation spectra of circular few electron quantum dots. *Science*, , no. 278, pp. 1788–1792.

Leburton, J.-P.; Nagaraja, S. (1997): *Electronic properties of Quantum dots and artificial atoms*, pp. 235–256. In Abstreiter, G., et al. Abstreiter, G., et al. (1997), 1997.

Lee, I.-H.; Rao, V.; Martin, R. M.; Leburton, J.-P. (1998): Shell filling of artificial atoms within density-functional theory. *Physical Review B*, vol. 57, no. 15, pp. 9035.

Likharev, K. K. (1995): Physics and possibles applications of single-electron devices. *FED*, vol. 6, pp. 5–14.

Macucci, M.; Hess, K.; Iafrate, G. (1993): Electronic energy spectrum and the concept of capacitance in quantum dots. *Physical Review B*, vol. 48, no. 23, pp. 17354–17363.

Macucci, M.; Hess, K.; Iafrate, G. (1995): Simulations of electronic properties and capacitance of quantum dots. *Journal of Applied Physics*, vol. 77, no. 7, pp. 3267.

Meir (1995): *Solid State Electronics*, vol. 34, pp. 1445.

Meirav, U.; Foxman, E. (1995): Single-electron phenomena in semiconductors. *Semiconductor Science and Technology*, vol. 10, pp. 255–284.

Meirav, U.; Kastner, M. A.; Wind, S. (1990): Single-electron charging and periodic conductances in gaas nanostructures. *Physical Review Letters*, vol. 65, no. 6, pp. 771–774.

Nagaraja, S.; Matagne, P.; Thean, V.-Y.; Leburton, J.-P.; Kim, Y.-H.; Martin, R. M. (1997): Shell-filling effects and coulomb degeneracy in planar quantum-dot structures. *Physical Review B*, vol. 56, no. 24, pp. 15752–15759.

Schmidt, T.; Haug, R.; von Klitzing, K.; Förster, A.; Lüth, H. (1997): Spectroscopy of the single-particle states of a quantum dot molecule. *Physical Review Letters*, vol. 78, no. 8, pp. 1544.

Slatter, J. (1972): *Advanced in Quantum Chemistry*, vol. 6, no. 1.

Sohn, L.L., et al.(Ed): *Mesoscopic Electron Transport*. Kluwer Academic Publisher.

Stopa, M. (1996): Quantum dot self consistent electronic structure and the coulomb blockade. *Physical Review B*, vol. 54, no. 19, pp. 13767–13783.

Tarucha, S.; Austing, D. G.; Honda, T. (1995): Resonant tunneling single electron transistors. *Superlattices and Microstructures*, vol. 18, no. 2, pp. 121–129.

Tarucha, S.; Austing, D. G.; Honda, T. (1997): Atomic-like properties of semiconductor quantum dots. *Japanese Journal of Applied Physics*, vol. 37, no. 6, pp. 3917.

Tarucha, S.; Austing, D. G.; Honda, T.; van der Hage, R. J.; Kouwenhoven, L. P. (1996): Shell filling and spin effects in a few electron quantum dot. *Physical Review Letters*, vol. 77, no. 17, pp. 3613–3616.

Tucker, J. R. (1992): Complementary digital logic based on the ‘Coulomb blockade’. *Journal of Applied Physics*, vol. 72, no. 9, pp. 4399–4413.

Wang, Y.; Chou, Y. (1993): Planar field-induced quantum dot transistor. *Applied Physics Letters*, vol. 63, no. 16, pp. 2257–2259.

Wasshuber, C.; Kosina, H.; Selberherr, S. (1998): A comparative study of single-electron memories. *IEEE Transactions on Electron Devices*, vol. 45, no. 11, pp. 2365–2371.

Zienkiewicz, O.; Taylor, R. L. (1994): *The Finite Element Method*. Mac Graw Hill.